Structure and Periodicities of Cross-Bridges in Relaxation, in Rigor, and during Contractions Initiated by Photolysis of Caged Ca^{2+}

Thomas D. Lenart,* John M. Murray,# Clara Franzini-Armstrong,# and Yale E. Goldman*
Pennsylvania Muscle Institute, *Department of Physiology and #Department of Cell and Developmental Biology, University of Pennsylvania, Philadelphia, Pennsylvania 19104 USA

ABSTRACT Ultra-rapid freezing and electron microscopy were used to directly observe structural details of frog muscle fibers in rigor, in relaxation, and during force development initiated by laser photolysis of DM-nitrophen (a caged Ca^{2+}). Longitudinal sections from relaxed fibers show helical tracks of the myosin heads on the surface of the thick filaments. Fibers frozen at ~13, ~34, and ~220 ms after activation from the relaxed state by photorelease of Ca^{2+} all show surprisingly similar cross-bridge dispositions. In sections along the 1,1 lattice plane of activated fibers, individual cross-bridge densities have a wide range of shapes and angles, perpendicular to the fiber axis or pointing toward or away from the Z line. This highly variable distribution is established very early during development of contraction. Cross-bridge density across the interfilament space is more uniform than in rigor, wherein the cross-bridges are more dense near the thin filaments. Optical diffraction (OD) patterns and computed power density spectra of the electron micrographs were used to analyze periodicities of structures within the overlap regions of the sarcomeres. Most aspects of these patterns are consistent with time resolved x-ray diffraction data from the corresponding states of intact muscle, but some features are different, presumably reflecting different origins of contrast between the two methods and possible alterations in the structure of the electron microscopy samples during processing. In relaxed fibers, OD patterns show strong meridional spots and layer lines up to the sixth order of the 43-nm myosin repeat, indicating preservation and resolution of periodic structures smaller than 10 nm. In rigor, layer lines at 18, 24, and 36 nm indicate cross-bridge attachment along the thin filament helix. After activation by photorelease of Ca^{2+}, the 14.3-nm meridional spot is present, but the second-order meridional spot (22 nm) disappears. The myosin 43-nm layer line becomes less intense, and higher orders of 43-nm layer lines disappear. A 36-nm layer line is apparent by 13 ms and becomes progressively stronger while moving laterally away from the meridian of the pattern at later times, indicating cross-bridges labeling the actin helix at decreasing radius.

INTRODUCTION

The conventional hypothesis for the mechanism of muscle contraction postulates that force production and filament sliding are accomplished via structural changes in the myosin cross-bridges as they interact with the actin filaments (Hanson and H. E. Huxley, 1955; A. F. Huxley, 1957; Reedy et al., 1965; H. E. Huxley, 1969). However, despite detailed knowledge of the structure of contractile proteins and their interactions (Milligan et al., 1990; Holmes et al., 1991; Rayment et al., 1993; Xie et al., 1994), the specific internal motions of the proteins that lead to contraction are still unknown.

A wealth of information has come from x-ray diffraction of whole muscles and single muscle fibers, especially during the onset of isometric tetanic contraction (Haselgrove and H. E. Huxley, 1973; Yagi et al., 1977; H. E. Huxley and Kress, 1985; H. E. Huxley et al., 1980, 1981, 1982; Kress et al., 1986; Amemiya et al., 1987; Bordas et al., 1991; Yagi, 1991; Wakabayashi and Amemiya, 1991; Harford et al., 1991). These studies have identified a sequence of events during activation including motions of the thin filament regulatory system, movement of cross-bridge mass toward the thin filaments and subsequent changes, probably related to actomyosin attachment and a power stroke that generates force or causes filament sliding. The x-ray diffraction technique provides high spatial resolution and is applicable to live muscle but is limited to detecting average or periodic structural information from a whole fiber or muscle. An approach that can allow study of selected areas of the sarcomere or individual cross-bridges is thus a necessary complement to x-ray diffraction in the detection of structural changes associated with contraction.

Rapid freezing of muscle fibers against a copper block at liquid helium temperature, followed by freeze substitution and electron microscopy, allows detection of structural details of active cross-bridges with good time and spatial resolution (Tsukita and Yano, 1985, 1986; Hirose and T. Wakabayashi, 1991; Craig et al., 1992; Suzuki et al., 1993; Hirose et al., 1993, 1994; Lenart et al., 1993; Sosa et al., 1994; Hawkins and Bennett, 1995). These experiments have shown preservation of the native structure to better than 10-nm resolution and have generally agreed that the cross-bridges in rigor muscle are well ordered (Tsukita and Yano, 1985, 1986; Hirose and T. Wakabayashi, 1991; Hirose et al., 1993; Lenart et al., 1993), but those present during active contractions have a highly variable shape and a wide angular distribution. Changes in cross-bridge shapes, related to

Received for publication 13 December 1995 and in final form 21 August 1996.

Address reprint requests to Dr. Yale E. Goldman, Pennsylvania Muscle Institute, University of Pennsylvania, Philadelphia, PA 19104-6083. Tel.: 215-898-4017; Fax: 215-898-2653; E-mail: goldmany@mail.med.upenn.edu.

Dr. Lenart's present address: Department of Ophthalmology, Mayo Clinic, Rochester, MN 55905.

0006-3495/96/11/2289/18 $2.00

functional states, have been detected by correspondence analysis of images from transverse sections (Hirose et al., 1994).

To obtain time resolution and to partly synchronize cross-bridge motions during force development, glycerol-extracted rabbit muscle fibers were previously studied using rapid freezing during the transition from rigor to active contraction initiated by photorelease of ATP from caged ATP. At early time points in those experiments cross-bridges were clearly a mixture of remaining rigor attachments and the early active ones (Hirose et al., 1993, 1994). Only limited x-ray diffraction data with this protocol are available for comparison (Brenner et al., 1989; Rapp et al., 1989; Poole et al., 1991).

In the studies presented here we used a protocol for rapid freezing and activation which gives data more directly comparable with those obtained by x-ray diffraction from electrically stimulated intact muscle, starting from the relaxed state, with all (or most) cross-bridges detached. Skinned frog muscle fibers were rapidly frozen in rigor, in relaxation, or at various times after laser photolysis of caged Ca^{2+} (Kaplan and Ellis-Davies, 1988). A comparison of x-ray diffraction data from live muscle with optical diffraction patterns or computed power density spectra of the electron micrographs (EMs) assists interpretation of the images. Many of the periodicities observed in the EMs correspond to those seen in x-ray diffraction experiments, but there are significant differences in certain reflections. Our results emphasize the appearance and strengthening of an actin-based periodicity more than the x-ray diffraction studies, suggesting attachment of cross-bridges in various configurations onto actin target zones and a recovery of myosin-based order in the process of tension production. Some of the data have been reported in preliminary form (Lenart et al., 1992, 1993; Murray et al., 1993).

MATERIALS AND METHODS

Preparation of muscle fibers

Sartorius muscles from *Rana temporaria* were dissected as described by Padrón and Huxley (1984), tested for excitability with a Grass S9 stimulator, and chemically skinned as in Magid and Reedy (1980). The muscles were dissected in Ringer's solution (115 mM NaCl, 2.5 mM KCl, 1.8 mM $CaCl_2$, 2.5 mM $MgCl_2$, 3 mM sodium phosphate buffer) at 2–4°C, immersed in a relaxing solution at pH 6.3 (5 mM Na_2ATP, 15 mM KPO_4 buffer, 75 mM potassium acetate, 5 mM magnesium acetate, 5 mM EGTA, 5 mM NaN_3, 2% polyvinylpyrollidone (PVP)) for 15 min, followed by a skinning solution, similar to relaxing solution but at pH 7.0 and containing 0.5% (v/v) of Triton X-100, for 3 h. Single fibers were dissected in the relaxing solution under silicone oil at 2–4°C.

Experimental set-up

Single skinned muscle fibers were mounted on a Cryo-Press freezing apparatus (Med-Vac, St. Louis, MO) (Heuser et al., 1979), interfaced to a pulse laser for photolysis of caged molecules and including facility to measure muscle fiber tension continuously through an experiment (see Hirose et al., 1993). Briefly, a single, skinned fiber was mounted by aluminum, T-shaped clips (Goldman and Simmons, 1984) between the hook of a tension transducer (Akers, AE801, Horten, Norway) and a stationary clamp attached to the freezing head. The fibers were mounted over an agar cushion on an aluminum planchet that could be easily removed from the device after freezing. Fibers were frozen by falling under gravity for ~200 ms and then impacting a gold-coated copper block cooled by liquid helium. Bounce was eliminated by the electromagnet, spring, and damped shaft system of the Cryo-Press.

A frequency-doubled ruby laser (Goldman et al., 1984) provided 50-ns (λ = 347 nm) pulses for photolysis. The laser beam was directed at the sample by a series of mirrors and checked for correct positioning by burn patterns on ultraviolet-sensitive paper (Kentek, Manchester, NH). The laser pulse was triggered at preselected times (13, 34, and 220 ms) before freezing. The degree of timing variability was ~2.5% at 20 ms and ~1% at 200 ms (Hirose et al., 1993).

Experimental procedure

The fibers were prepared for photolysis and freezing by exchange with a series of solutions for 2 min each using a set of stirred solution wells that maintained the temperature at 2–6°C (Hirose et al., 1993). The fiber was rinsed twice in the pH 7.0 relaxing solution listed above, then in a 3 mM ATP relaxing solution (3 mM Na_2ATP, 0.66 mM $MgCl_2$, 0.5 mM EGTA, 1.84 mM 1,6-diaminohexane-*N*,*N*,*N*′,*N*′-tetraacetic acid (HDTA), 100 mM *N*-tris(hydroxymethyl) methyl-2-aminoethane-sulfonic acid (TES), 29.5 mM creatine phosphate (CP), 2 mM glutathione (reduced form, GSH), 2% PVP, and two exchanges of a preactivating solution (3 mM Na_2ATP, 1.2 mM $MgCl_2$, 0.1 mM EGTA, 1.84 mM HDTA, 100 mM TES, 20 mM CP, 10 mM GSH, 2% PVP). The fiber was then transferred to caged calcium solution (Kaplan and Ellis-Davies, 1988) (1.94 mM DM-nitrophen, 1.6 mM $CaCl_2$, 3 mM Na_2ATP, 1.2 mM $MgCl_2$, 25.7 mM HDTA, 100 mM TES, 20 mM CP, 10 mM GSH, 2% PVP). Typically, this photolysis solution, providing a calculated free $[Ca^{2+}]$ of 250 nM, poised the fiber at the threshold of the pCa-tension curve or activated the fiber slightly (1–2% of fully active tension). Occasionally, the $CaCl_2$ concentration was adjusted up or down from this value.

For obtaining the structure in rigor, the fiber was transferred from 5 mM ATP, pH 7.0, relaxing solution to a rigor solution containing 100 mM TES, 34 mM EDTA, 2% PVP, pH 7.0, at 2–4°C. After rigor tension developed and stabilized the fiber was rinsed once or twice more in the rigor solution.

When the fiber was equilibrated with the final solution for a freezing run, excess solution was removed by aspiration with a small cannula and the freezing head with mounted fiber was transferred to the Cryo-Press. The temperature of the fiber was then approximately 10°C.

Electron microscopy

The samples were freeze substituted with 0.1–0.5% tannic acid in acetone at −80°C for 2 days, warmed to −20°C for 3 h, rinsed in acetone three times for 10 min each at −20°C, transferred to 4.0% OsO_4 in acetone, and then warmed to room temperature over a ~2-h period. In some experiments, the freeze substitution was conducted without tannic acid (only Fig. 2 *B* here). The samples were rinsed in acetone three times for 10 min each, stained en bloc with 1% uranyl acetate in acetone for 3 h, rinsed in acetone briefly or overnight, and embedded in araldite. Sections were cut tangent to the frozen surface, with the knife edge perpendicular to the filament axis. Sections were stained with uranyl acetate and lead citrate and examined in a Phillips EM410 electron microscope. All measured periodicities are approximated to the nearest known period.

Image analysis

Digitization and calculation of power spectra

EMs of longitudinal sections were selected for processing by examination of their optical diffraction patterns. Astigmatic or inappropriately focused micrographs were discarded. Regions that appeared reasonably well or-

dered by optical diffraction were digitized, using a Perkin-Elmer model 1010G microdensitometer, on a raster corresponding to 2 nm at the specimen for images taken at a magnification of ×24,400 or 2.5 nm for images at ×10,200. As we were primarily interested in the cross-bridges, all areas of the images outside the regions of overlap between the thick and thin filaments were masked out. The individual overlap zones were then extracted into separate, small sub-images for calculation of the Fourier transforms and power spectra (computed diffraction pattern). All calculations were carried out using the Semper image processing system (Synoptics, Cambridge, UK) on a Sun 4/330 computer.

To enhance the signal-to-noise ratio in our computed diffraction patterns, we added together the power spectra from many different overlap zones at each time point. For this purpose, the sub-images were all rescaled to the same magnification and rotationally aligned. In addition, the compression and shearing due to thin sectioning were individually corrected in each image. We used the meridional reflection at ~14 nm in the diffraction patterns as an internal magnification calibration and to define the meridional direction. The equator is always very intense, so the equatorial direction is easily defined. These two directions plus the internal magnification calibration are sufficient to calculate vectors for a new coordinate system for each sub-image so that a single interpolation simultaneously rescaled it to the standard magnification, rotated it to make the equator horizontal, and sheared it to make the meridian perpendicular to the equator. The power spectra of the corrected images were then added together. The meridional spacings of all intensities are approximated to the nearest known x-ray reflection.

Difference spectra

Difference diffraction patterns between states were obtained by subtracting summed power density spectra, after normalizing to compensate for factors that lead to random variations in image contrast and intensity in the power spectra (e.g., variations of specimen thickness, degree of staining, microscope defocus and objective aperture settings, and film development). For normalization we used the most straightforward assumption, that the total scattering per unit cell remains constant throughout the changes in the physiological state. This assumption implies that the sum of the intensities of all the pixels in the power spectra should be constant. Intensities outside the calculated power spectra would make only a small contribution to this sum. All of the power spectra had the same number of pixels, so we simply scaled the intensities of each summed power spectrum to adjust the mean intensity to a value of 100.

Minor errors in normalization and distortion between the axial and lateral spacings prevent the difference power spectra from being reliable for precise quantitative statements on intensity changes. However, they are useful for visualizing the large differences that are obvious in the patterns, and they are very sensitive to changes in the positions of layer line maxima.

RESULTS

Relaxed muscle

As in previous work (Heuser et al., 1979; Craig et al., 1992; Hirose et al., 1993), we find a region of fiber, within a depth of approximately 10 μm from the freezing surface, that shows good freezing with no evidence of ice crystal damage. Fibers frozen in the relaxed state exhibit sarcomeres of uniform length that are straight and aligned laterally (Fig. 1). The edges of the A band and the H zone (nonoverlap region of the thick filaments) are sharp, indicating that both thick and thin filaments are also laterally well aligned. The thick filaments show some bowing, resulting in a slight barrel distortion of the A bands (M lines are wider than the A-I junctions). The thin filaments in the I bands of relaxed fibers are often wavy.

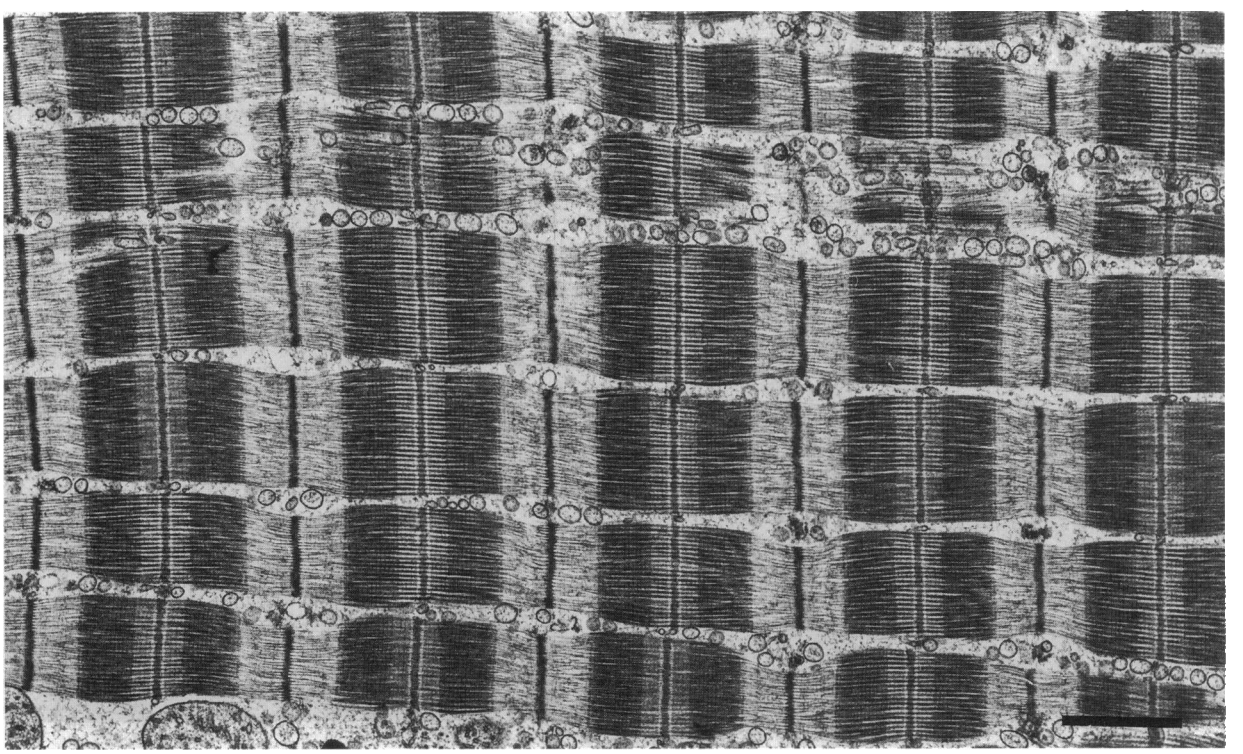

FIGURE 1 Longitudinal section of a rapidly frozen, relaxed frog sartorius muscle fiber. The sarcomeres are straight, well aligned, and uniform in length. Bar, 1.0 μm.

At higher magnification, helical periodicities are prominent on the surface of the relaxed thick filaments, particularly in images with contrast enhanced by treatment with tannic acid (Fig. 2 *A*, slanted arrows). The helical tracks are due to myosin heads slewed around the thick filament axis (Kensler and Stewart, 1986, 1989; Cantino and Squire, 1986; Heuser and Cooke, 1983). The apparent diameter of thin and thick filaments is increased by tannic acid treatment, and this reduces the interfilament spaces, making it difficult to distinguish the borders of the thick and thin filaments in the overlap zone. In the nonoverlap (H) zone very few, if any, myosin heads project out from the surface of the thick filaments. When fibers are freeze substituted in the absence of tannic acid, filament diameters are smaller and the interfilament space is clearer (Fig. 2 *B*). Very few myosin heads cross the space between the thick and thin filaments in these images and the lateral edges of the filaments are clearly distinguishable. Note that the slew of the myosin heads on the surface of the thick filaments is evident albeit less prominent than in samples treated with tannic acid.

In thicker sections from relaxed fibers (Fig. 3 *A*), the A bands show the 11 transverse lines at a 43-nm repeat on each side of the bare zone that are thought to arise from the periodicity of thick filament accessory proteins (C, X, H, or F proteins; Pepe and Drucker, 1975; Craig and Offer, 1976; Bennett et al., 1986). The weaker transverse lines in the lateral third of the A band are presumably due to myosin

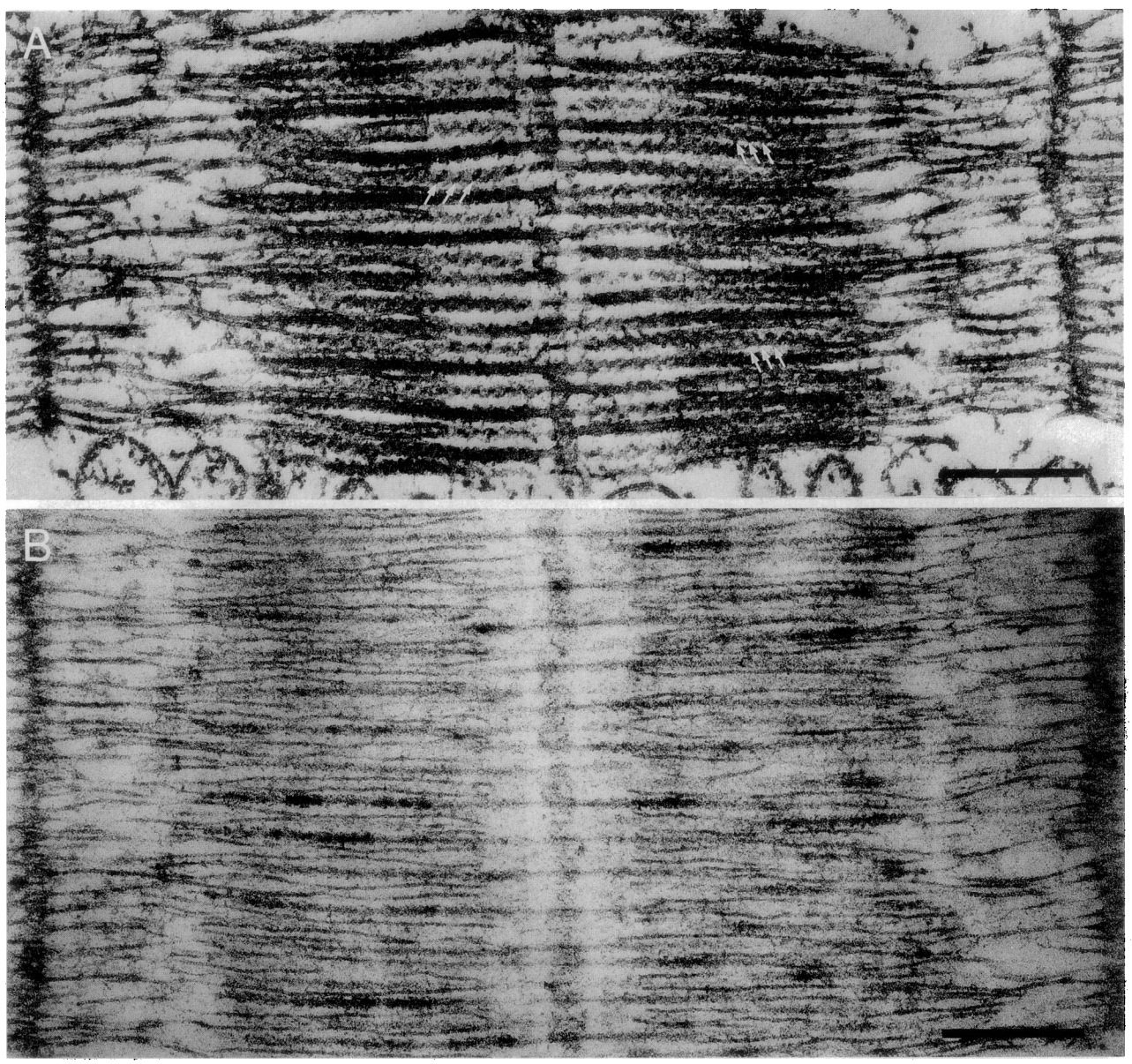

FIGURE 2 Higher magnification views of frog fibers frozen in relaxing solution and freeze substituted in the presence (*A*) or absence (*B*) of tannic acid. The tannic acid makes the filaments in *A* appear larger in diameter than in *B*. Helically arranged, relaxed myosin heads are visualized in *A* by glancing in the direction of the white arrows. In *B*, the thin filament edges are smooth, indicating that cross-bridges are not attached. Bars, 0.25 μm.

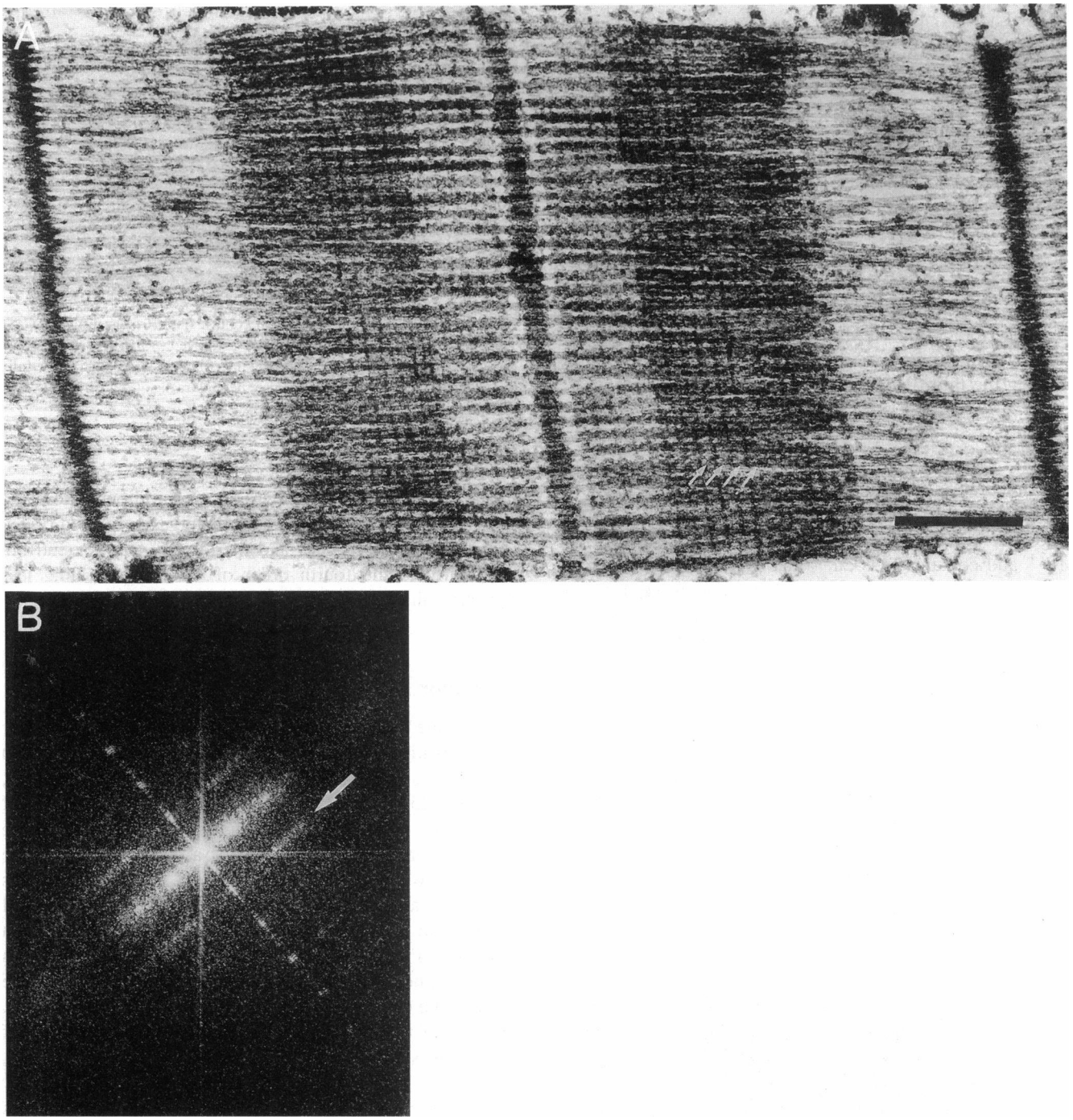

FIGURE 3 Micrograph of a relaxed sarcomere (*A*) and the optical diffraction pattern (*B*) of an overlap zone from this image. In this thicker section, cross-banding with 43-nm spacing is visible due to the accessory proteins. The slanted arrows point to helical tracks due to myosin heads. Bar, 0.25 μm. In *B*, the myosin meridional spots extend out to six orders of 43 nm (*arrow*).

heads helically ordered at 43 nm. An oblique periodicity with the same axial spacing is indicated by white slanted arrows in Fig. 3 *A* and can be seen by sighting along the arrows while viewing the micrograph at a shallow angle.

Optical diffraction patterns from electron micrographs of relaxed overlap zones show meridional spots extending to the fourth order of the 43-nm periodicity (approximately 11 nm) and sometimes to the fifth or sixth order (9 and 7 nm; Fig. 3 *B*). The meridional spot at 22 nm, the second order of 43 nm, is as intense as the first and third meridional intensities (43 and 14.3 nm, respectively). Layer lines indexing on 43 nm are detectable to the fourth or fifth order (9 nm). These results indicate that the rapid freezing, freeze-substitution technique preserves periodic structures to a resolution of at least 7.2 nm, but it can be argued that the preservation of nonperiodic structures is better (Hirose et al., 1993).

Rigor

In rigor fibers, thin filaments are straight (Fig. 4) and the edges of the myofibrils are slightly scalloped, the diameter of the overlap zones being smaller than that of the Z lines and the M bands. As expected, the overlap region is quite different from that in relaxed fibers, due to the ordered arrangement of cross-bridges. In the H zone, the myosin heads extend out into the interfilament space without any apparent order (Fig. 4; see also Padrón and Craig, 1989). A transverse periodicity is obvious in the overlap region, but it has different characteristics from that seen in relaxed sarcomeres. The 43-nm periodicity is replaced by domains of strong periodicity at 36 nm separated by areas of apparent disorder. The 36-nm periodicity is expected of cross-bridges labeling the thin filament helix.

Pre-flash controls

The first step in the photolysis experimental protocol is to equilibrate the fibers in a solution containing DM-nitrophen (caged Ca^{2+}). The caged Ca^{2+} solution is very low in free Mg^{2+} and contains free Ca^{2+} that poises the muscle fiber just below the threshold of the pCa-tension curve. Little or no tension development was observed in solutions containing 2 mM DM-nitrophen and 1.6 mM total $CaCl_2$, leading to a calculated free [Ca^{2+}] of 250 nM.

In fibers frozen in the caged Ca^{2+} solution (pre-flash control) the helical periodicity of the thick filaments, in both the overlap and nonoverlap regions (Fig. 5, oblique arrows), and the 43-nm transverse lines in the central A band are preserved (transverse arrows). However, despite maintaining a helical arrangement, the myosin heads in the H zone extend into the interfilament space to a greater extent than is seen for the fully relaxed fibers, as if the low [Mg^{2+}] or elevated [Ca^{2+}] diminish the extent of cross-bridge relaxation. Diffraction patterns of the overlap zones of pre-flash caged Ca^{2+} fibers (not shown) show meridional spots and layer lines indexed on a 43-nm spacing, as in relaxed fibers. However, the layer lines and meridional spots extend out maximally to the fourth order of 43 nm, indicating less regularity than in relaxing solution.

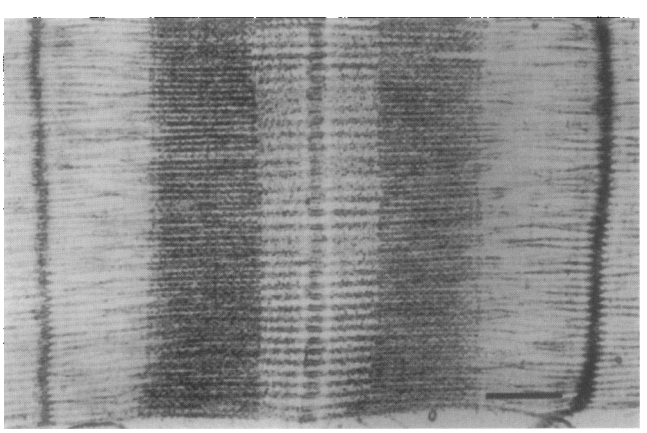

FIGURE 4 Micrograph of a sarcomere in the rigor state. The thin filaments are straighter than in relaxed fibers. There is minor scalloping of the myofibril edges in each half-sarcomere. Cross-banding is best visualized by glancing across the A band at a shallow angle. It has a different periodicity from that of relaxed muscle. Bar, 0.25 μm.

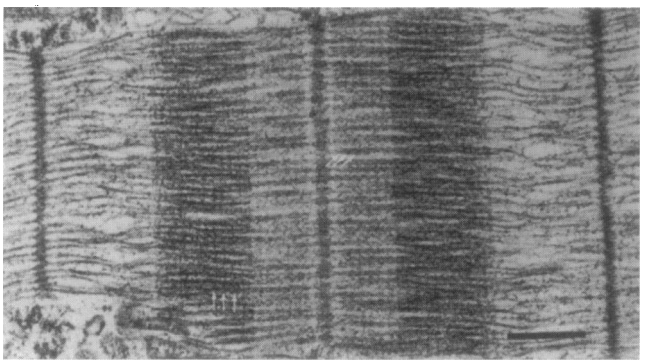

FIGURE 5 Image from a pre-flash control fiber, frozen in caged Ca^{2+} solution. The 43-nm transverse lines are preserved (*transverse arrows*), but the myosin heads extend more into the interfilament space than in the fully relaxed fibers. Oblique arrows indicate helical tracks of myosin heads. Bar, 0.25 μm.

Activation

To examine the time course of structural changes that occur after activation by photorelease of Ca^{2+}, fibers were frozen at 12–15 ms (average, 13 ms), 31–34 ms (average, 34 ms), and 210–230 ms (average, 222 ms) after photolysis of caged Ca^{2+} while continually monitoring tension. Force began to rise within 1–2 ms after a laser pulse and rose smoothly to a plateau. At 13, 34, and 220 ms, the fibers developed approximately 15, 45, and 100% of the full steady-state active tension, respectively (see inset tension records of Figs. 6 and 7). These relative tension estimates were obtained by averaging the tension achieved at the earlier time points in traces from fibers frozen at 220 ms. The rate of tension development is consistent with that of intact frog sartorius muscle at 10°C (H. E. Huxley et al., 1982).

In fibers frozen 13 ms after the laser pulse (Fig. 6), densities (presumably cross-bridges) extend from the thick to the thin filaments in the overlap region. Many of the cross-bridges are perpendicular to the filament axis, but there is a variety of angles, with some tilted toward and some tilted away from the M line. The helical arrangement of the myosin heads on the surface of the thick filaments is sometimes still visible in the H zone (Fig. 6, tilted arrow), but this periodicity is weaker than in the relaxed fibers and pre-flash controls. The 43-nm transverse lines crossing the whole sarcomere are absent; however, microdomains with short stretches of transverse lines, corresponding to the positions of cross-bridges, can be seen by glancing across overlap regions in the A band. The exact spacing between these lines is difficult to measure directly

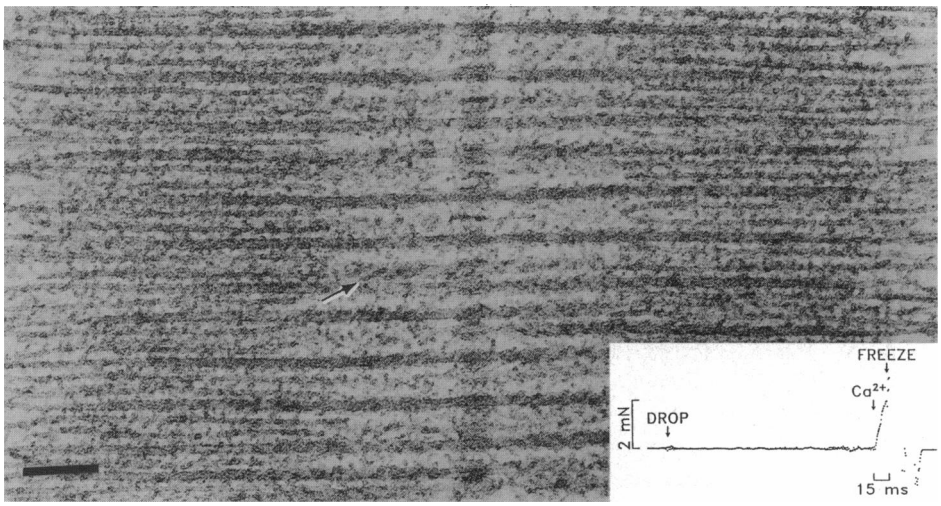

FIGURE 6 Force recording (*inset*) and EM of a frog fiber frozen 15 ms after photolysis of caged Ca^{2+}. The plunger rod of the freezing apparatus was released at the time indicated by DROP. At Ca^{2+}, the laser pulse was triggered, liberating 1.8 mM free Ca^{2+} by photolysis of DM-nitrophen and tension rose sharply. At FREEZE, the fiber contacted the cryogenic metal surface. The resultant image shows many densities extending from the thick filament to the thin filament (presumably cross-bridges) with a variety of shapes and angles. Some helical arrangement of the myosin heads is still apparent in the H zone. This can be visualized by glancing in the direction of the arrow. Bar, 0.1 μm.

from the micrographs but is obtained from the computed power density spectra described below.

Images from fibers frozen at 34 and 220 ms after activation still show highly ordered sarcomeres, with good lateral alignment (Fig. 7, frozen at 220 ms). There is less barrel distortion than in relaxed fibers, but the edges of the A band and H zone are less sharply delimited, and the M line is less straight, indicating some longitudinal shift of the filaments.

At higher magnification, the shapes and angles of cross-bridges at plateau isometric tension are similar to those in fibers frozen at 15 or 45% of the plateau tension (Fig. 8). The density of the cross-bridges is uniform across the space between the two sets of filaments. Cross-bridges are often perpendicular to the filament axis but show considerable variation in angle. As at earlier time points, transverse periodicities, coinciding with the positions of cross-bridges, are visible over small areas, often as sets of double lines (Fig. 8). In contrast to the images before and just after activation, however, helical tracks on the thick filaments are not visible in the H zone.

Summed power spectra

To improve the signal-to-noise ratio of the computed diffraction patterns, EMs were digitized and the power density spectra from Fourier transforms of multiple images were summed. For this analysis we selected multiple (40–113) overlap regions from fibers in each physiological state. The procedure for scaling and aligning the power spectra before the summation is described in Materials and Methods. The resulting power spectra correspond to optical diffraction patterns averaged over many overlap zones. In all patterns we use the third meridional spot as a reference for spatial frequencies and assign it a position at 14.3 nm. Tables 1 and 2 provide a qualitative indication of the relative intensities of the various meridional spots and layer lines.

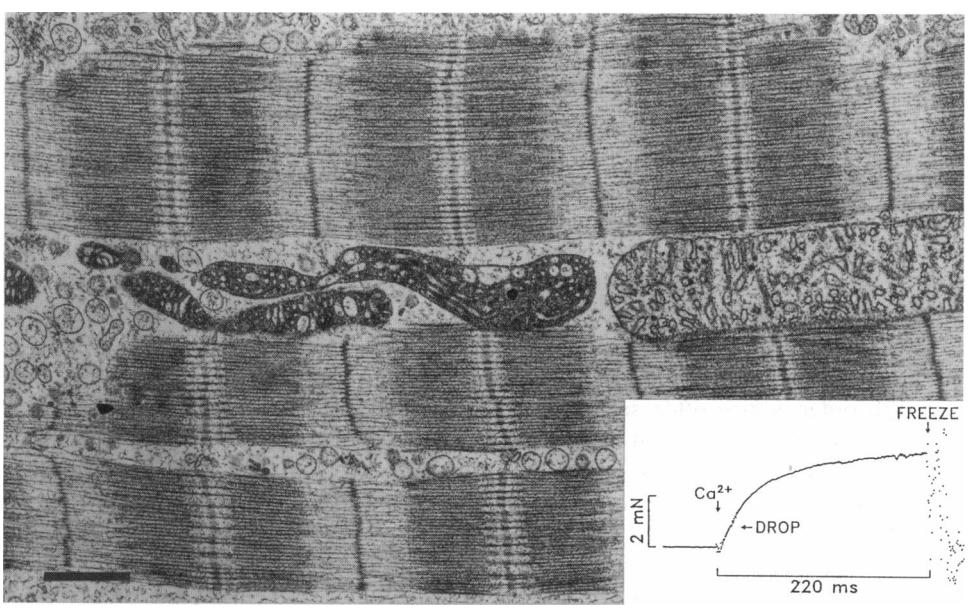

FIGURE 7 Force recording (*inset*) and EM of a fiber frozen at the plateau of isometric contraction. The laser was triggered at the time point indicated by Ca^{2+}, releasing 0.6 mM free Ca^{2+}. At DROP, the plunger rod was released, and at FREEZE, the fiber contacted the cold metal block. The time between the laser pulse and the freezing was 220 ms. There is less barrel distortion of the sarcomeres in this fully activated fiber compared with relaxed and rigor muscles. Irregularities of the M lines indicate minor longitudinal shifting of the thick filaments. Bar, 0.5 μm.

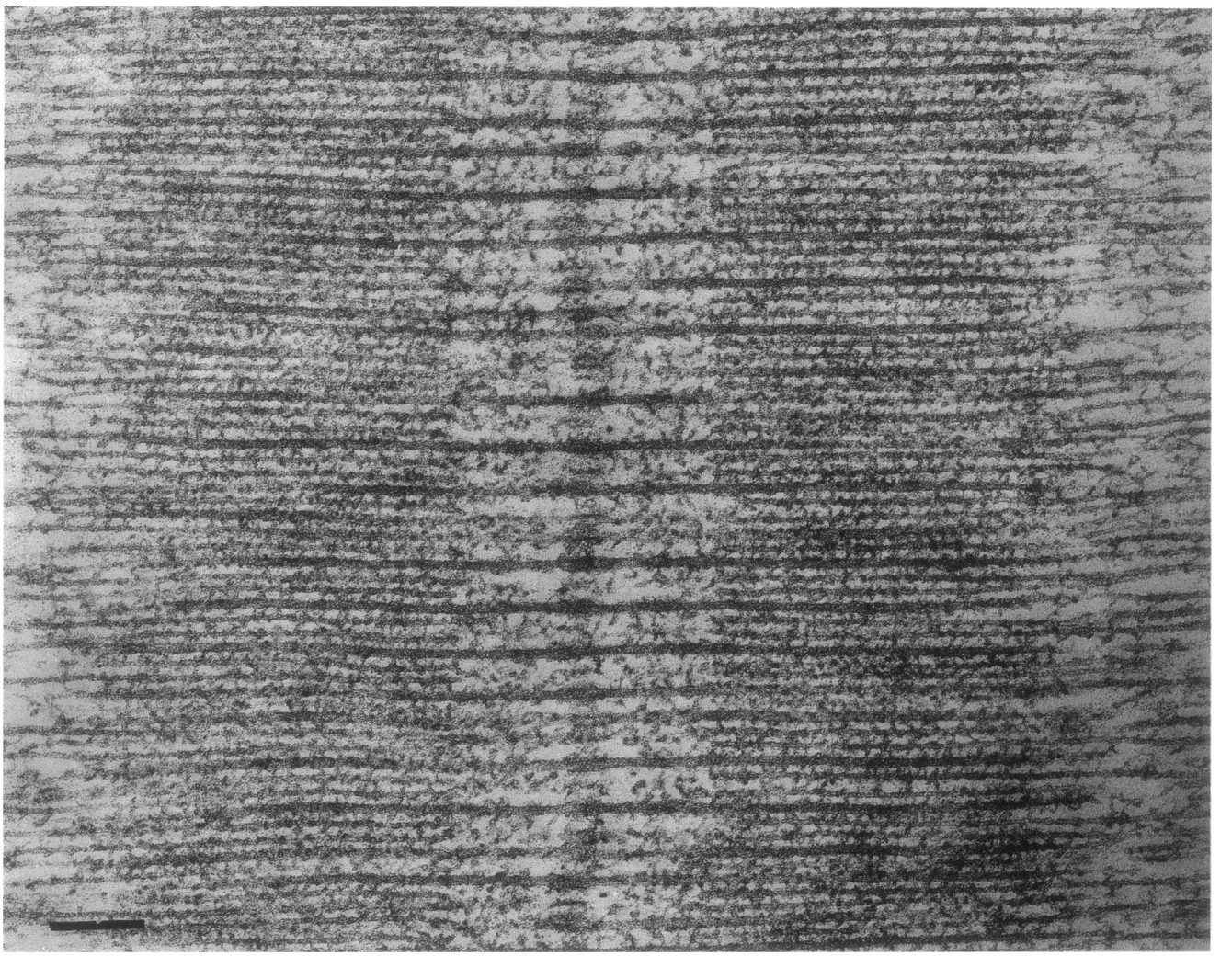

FIGURE 8 High-magnification image of a sarcomere from a fiber in steady isometric contraction. Cross-bridge shapes and angles are highly variable. Transverse periodicities are still apparent across the sarcomere. Myosin heads are very disordered in the H zone. Bar, 0.1 μm.

The relaxed power density spectrum (Fig. 9 *A*) is dominated by the thick filament periodicities at spacings indexing on 14.3 nm, as in the individual optical diffraction patterns (Fig. 3 *B*). The most prominent intensities are the meridional spots at 43, 36, 22, and 14.3 nm and the layer lines at 43 and 22 nm. The region of the meridian between 30 and 50 nm is complex with several (four or more) maxima. The second meridional spot cluster (near 22 nm) is similarly complex. Layer lines at 43 and 22 nm are prominent. A faint layer line is present at 19 nm with a corresponding meridional spot.

In the best power spectra from a single A band (Fig. 9 *B*), four orders of the 43-nm meridional intensity are visible. A faint fifth order is also often seen (off-scale in Fig. 9 *B*). Fewer orders appear in the summation for averaged power density spectra than in the best optical diffraction patterns. The probable explanation for this difference is that, relative to the layer lines, the strength of the meridional spots is quite variable because they are much more sensitive to orientation of the filament axes with respect to the plane of sectioning. Slight variations in orientation of our sections often dimmed the meridional spots without significantly affecting the layer lines, leading to reduced intensity of the meridional spots in the averaged power spectra.

The average power spectrum for pre-flash fibers (not shown) is similar to the relaxed pattern but with evidence of less order. The meridional spots and layer lines characteristic of relaxed muscle, such as the myosin-based reflections, are present but less intense. As in relaxation, we did not observe a 36-nm layer line in this state.

The average power spectrum for the overlap zones from rigor fibers (Fig. 9 *C*) is clearly different. The first and third meridional spots (43 and 14.3 nm) derived from thick filament periodicities are clear, but the second (22 nm) is absent. The first meridional spot has a single maximum at 43 nm. A strong layer line at 36 nm and a weak one at 18 nm (arrows in Fig. 9, *C* and *F*) are present due to cross-bridges tagging the helical structure of the thin filaments. A layer line at 24 nm is consistent with sampling of the actin helix by the myosin 14.3-nm periodicity ($1/14.3 - 1/36 \approx$

TABLE 1 Relative intensities of the main meridional spots

Axial position (nm)	Relaxed	13 ms	34 ms	220 ms	Rigor
14.3	W	W	S	S	S
22	S	W	W	W	–
36 (38*)	S	W*	S*	S*	–
43	S	W	S	S	S

For each condition or time after Ca^{2+} release, the meridional intensities were scored qualitatively for intensity. –, not appreciable; W, weakly visible; S, high intensity.
*Spots were measured to be at 38 nm.

TABLE 2 Peak radial positions and intensities of the main layer lines

Axial position (nm)	Relaxed	13 ms	34 ms	220 ms	Rigor
14.3	–	–	29 B	–	24W
22	43B	B*	38W	31W	–
36 (38*)	–	57B#	45W	24 S	28 V
43	23S	43W	38W	36 S	28B§

Numbers in the body of the table give the approximate radial reciprocal positions of the peak layer line intensities in nanometers. For each condition or time after Ca^{2+} release, the layer lines were also scored qualitatively for intensity. –, not appreciable; B, barely visible; W, weakly visible; S, strongly visible; V, very strong.
*The layer line is visible but too noisy for the lateral position to be determined reliably.
#The layer line was located at 38 nm axial spacing.
§The layer line may be intensity spread from the very strong 36-nm layer line rather than an independent intensity.

1/24). There is a clear myosin layer line at 14.3 nm, but the 43-nm layer line is only faintly visible or absent. These changes are consistent with loss of the myosin helical order and cross-bridge labeling of actin target zones (Huxley and Brown, 1967; reviewed by Haselgrove, 1983).

The power density spectra of Fig. 9, *D–F*, show the progression of structural features at 13, 34, and 220 ms after release of Ca^{2+} from the relaxed state. Shortly after photorelease of Ca^{2+} (Fig. 9 *D*, 13 ms), features of the relaxed power density spectrum are weaker but still visible, particularly the meridional spots at the first, second, and third orders of 43 nm. The first- and second-order myosin layer lines, at 43 and 22 nm, are also present but weaker than in relaxation. A new feature is the appearance of a weak layer line at 38 nm. As both 43- and 38-nm layer lines are present in the power spectrum, the microdomains of transverse lines in the images noted earlier (e.g., Fig. 6) probably represent both periodicities. There is a very weak layer line and a meridional spot at 19 nm.

Summed power spectra from images of fibers frozen at 34 ms (Fig. 9 *E*) and 220 ms (Fig. 9 *F*) after Ca^{2+} release show progressive increase of the intensities at the first- and third-order myosin meridional spots (43 and 14.3 nm). The second-order meridional spot (22 nm) remains weak. A meridional spot at 38 nm becomes increasingly distinct at 34 and 220 ms. At 220 ms, a spot is also detectable on the meridian at 57 nm.

Layer line intensities at 36 and 43 nm increase progressively. The layer line doublet at these two spacings is clearly visible in optical diffraction patterns from single A bands (Lenart et al., 1993). At 13 ms a weak layer line is located at approximately the same 38-nm axial position as the meridional spot, but at 34 and 220 ms, the axial spacing of the growing layer line is at 36 nm, distinct from the 38-nm meridional spot. This difference can be appreciated by sighting across the patterns in Fig. 9, *E* and *F*. The second-order myosin-based layer line (at 22 nm) becomes more visible at 34 ms and prominent at 220 ms. A layer line at 19 nm increases in intensity and a separate 18-nm layer line becomes visible at 220 ms. The mixed actin-myosin reflection at 24 nm seen in the rigor pattern is not appreciable as a distinct layer line at 220 ms. However, based on the ratio of the 24-nm to the 36-nm layer line strengths in rigor and the 36-nm layer line strength at 220 ms, the expected intensity on the 24-nm layer line in active contraction would be smaller than the noise due to random scatter.

The lateral distances of the layer line maxima away from the meridian vary among the states (Table 2). Between 13 and 220 ms, the peak intensity along the 36-nm layer line moves outward laterally from the meridian, indicating mass around actin moving closer to the filaments (see Table 2). The shift of the 36-nm layer line between 34 ms (Fig. 9 *E*) and 220 ms (Fig. 9 *F*) is very noticeable in comparison with the 43-nm layer line, which shifts very little during this time interval. The lateral position of the peak for the 36-nm layer line in rigor is similar to that in the 220-ms pattern.

On activation, the early loss of intensity of the 43-nm layer line is away from the meridian, so the peak position at 13 ms is closer to the meridian than in relaxation. The position of the 43-nm layer line peak shifts away from the meridian between 13 ms (Fig. 9 *D*) and 34 ms but by less than the 36-nm peak. A value is shown in Table 2 for the lateral position of the 43-nm layer line in rigor, but the intensity might arise from overlap of the strong 36-nm layer line rather than as an independent line. In relaxation the 43-nm layer line is clearly further from the meridian than during contraction, indicating a smaller radius of mass around the thick filament.

Difference power density spectra

The summed power density spectra were scaled in total intensity and then differences between pairs were calculated to emphasize changes of intensity and position of peaks during the onset of contraction and differences between relaxed and rigor muscles (Fig. 10). As discussed in Materials and Methods, the difference power spectra are mainly useful for visualizing large intensity differences between patterns, and they are very sensitive to changes in the positions of layer line maxima.

The rigor minus relaxed subtraction (Fig. 10 *A*) shows the changes in the power density spectrum caused by loss of myosin-based order, which predominates in relaxation, and acquisition of actin-based periodicities, as cross-bridges label the actin target zones in rigor. Yellow and red colors indicate increased intensity in rigor relative to relaxation;

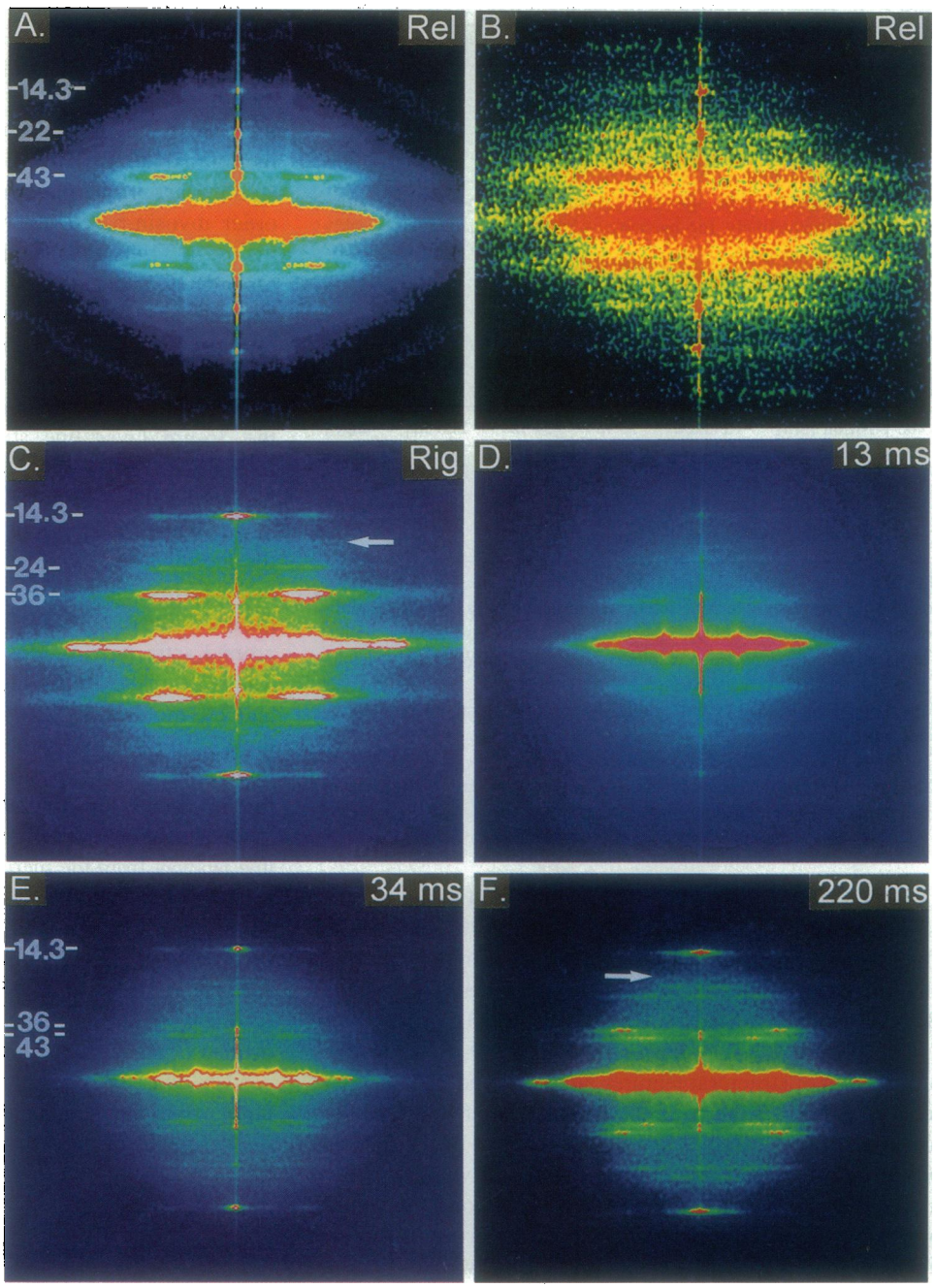

FIGURE 9 Summed power spectra from Fourier transforms of multiple images of overlap zones. The summed power spectra are derived from 102 overlap zones from relaxed fibers (*A*), 40 from rigor fibers (*C*), 96 at 13 ms after activation (*D*), 44 at 34 ms after activation (*E*), and 113 overlap zones at 220 ms after activation (*F*). (*B*) The power spectrum from a single, relaxed overlap region. For each pattern the look-up table for the display was adjusted to match the dynamic range of the data. Positions of the major layer lines are indicated. The arrows in *C* and *F* point to the 18-nm layer line.

black indicates a decreased intensity. The features that are stronger in rigor are the first actin layer line (at 36 nm, not detectable in relaxed patterns), the layer line at 24 nm (arrowhead), and the third-order meridional spot and layer line (at 14.3 nm). The main features that are stronger in the relaxed pattern (black in Fig. 10 *A*) are the first- and second-order meridional spots (at 43 and 22 nm, both showing evidence of complexity), and the first myosin layer line at 43 nm. The decrease of intensity on the 43-nm layer line is partly masked by the increase at 36 nm. Changes in many of the less intense spots and layer lines when the muscle is put into rigor are also evident in Fig. 10 *A*. The 18-nm layer line is stronger in rigor. It appears as a diffuse yellow intensity, more prominent in the subtracted pattern than in the rigor pattern alone. The 22-nm layer line is stronger in the relaxed pattern (and thus appears black).

The difference patterns between activated and relaxed muscle show that the myosin-based and actin-based periodicities change during activation with different time courses. In these difference power density spectra (Fig. 10, *B–D*), features that increase in intensity with time are shown in yellow and red and those that decrease are black. The

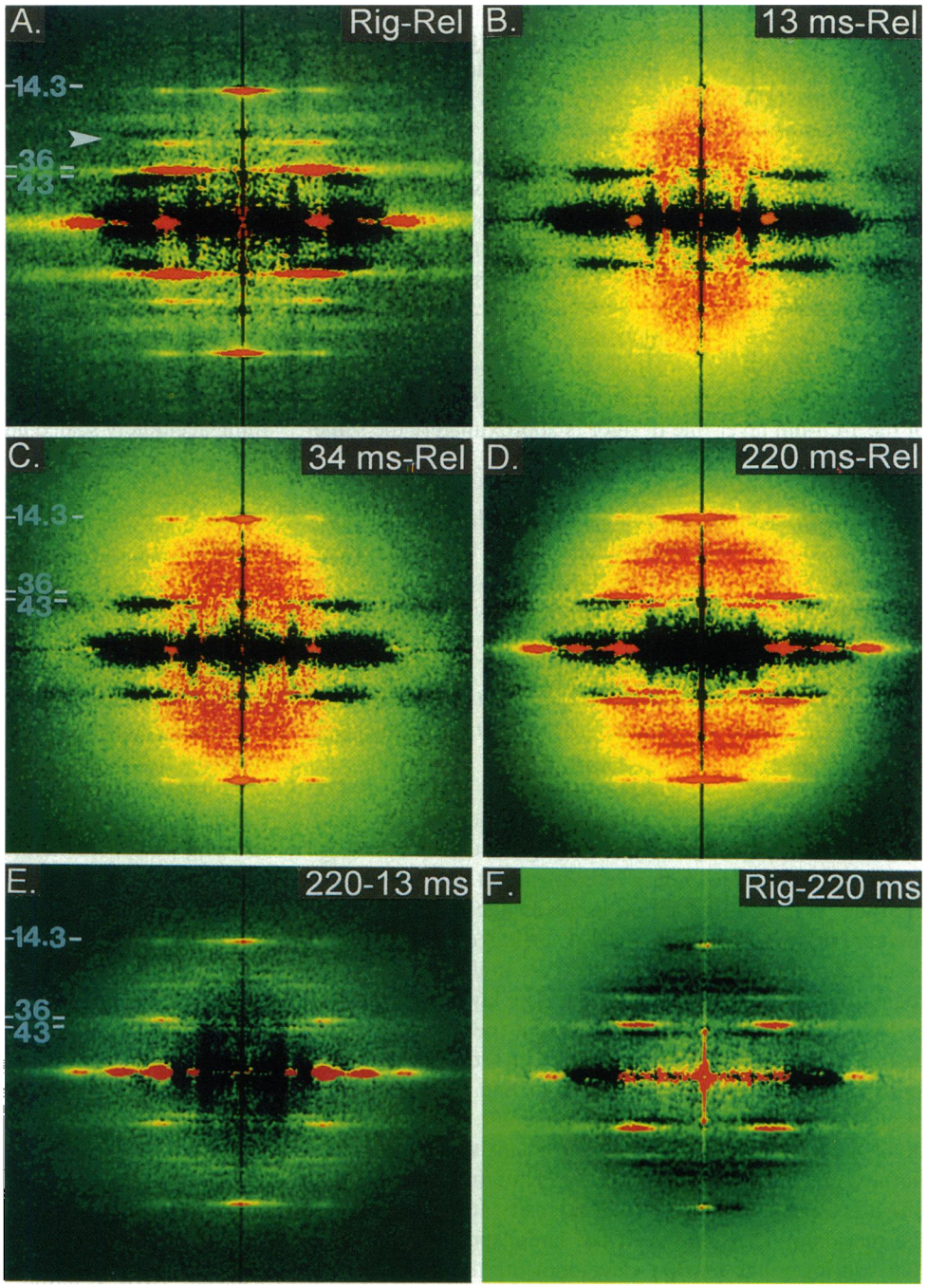

FIGURE 10 Difference power density spectra. Summed power density spectra were scaled to equalize the mean intensity and then subtracted. The differences shown are: rigor minus relaxed (*A*), 13 ms minus] relaxed (*B*), 34 ms minus relaxed (*C*), 220 ms minus relaxed (*D*), 220 ms minus 13 ms (*E*), and rigor minus 220 ms (*F*). Yellow and red colors indicate higher pixel values and black indicates lower pixel values in each difference spectrum. For example, in *A*, the bright red layer line labeled 36 nm indicates higher intensity in rigor than in relaxation.

myosin-based periodicities initially decrease markedly and later recover. Actin-based intensities appear shortly after Ca^{2+} release and then strengthen progressively. Changes in the 14.3-nm meridional spot are striking, increasing markedly during later tension development. Intensities on the meridian closer to the equator than the 14.3-nm spot are weaker throughout contraction than in relaxation (Fig. 10, *B–D*). Layer lines at 14.3, 18, 19, 22, and 36 nm intensify with time. The behavior of the 43-nm layer line in difference patterns is complex due to lateral shifts and is described later.

The difference pattern between early and late active time points (Fig. 10 *E*, 220 minus 13 ms) shows an overall increase in intensity of both actin- and myosin-based reflections (all of which are shown as yellow or red), except for the first- and the second-order meridional spot clusters.

In the difference pattern of rigor minus 220 ms (Fig. 10 *F*), the rigor layer lines at 36 and 24 nm and the 14.3- and 43-nm meridional spots are stronger (yellow or red). The 220-ms pattern, on the other hand, has more intensity on the 43-nm layer line and for three closely spaced lines at 18, 19,

and 22 nm, leading to black areas in the difference pattern. Thus, some of the myosin periodicities lost at early times in active contraction but regained by 220 ms are weak in rigor muscle and some actin-based periodicities are stronger in active contraction than in rigor.

The difference patterns are sensitive to lateral position of the layer lines and to shifts in those positions (see also Table 2). Fig. 10 *A* shows clearly that the positions of peak intensities along the 36- and 24-nm layer lines in rigor (red color) are located at a smaller lateral distance from the meridian than the 43- and 22-nm layer lines of the relaxed patterns (black), presumably reflecting the very tight association of the heads with the thick filament backbone in relaxation. The lateral position of the increased contribution of the 14.3-nm layer line in rigor is approximately the same as that of the 36- and 24-nm lines.

Comparing rigor with fully active muscle (Fig. 10 *F*), the lateral positions of the 18-, 19-, and 22-nm layer lines, more intense in the 220-ms pattern (black in Fig. 10 *F*), are closer to the meridian compared with that of the rigor 24-nm layer line, which is yellow. The intensity increase at 36 nm in rigor compared with 220 ms is farther from the meridian than the decreased intensity on the 43-nm layer line. The small lateral shift of the 36-nm layer line between active and rigor muscle (Table 2) is masked by the very high intensity in rigor.

In active muscle compared with relaxed (Fig. 10, *B–D*), the intensity along the 43-nm layer line increases at small lateral distances (particularly at 34 (Fig. 10 *C*) and 220 (Fig. 10 *D*) ms), but there is loss of intensity at a larger lateral distance. In the 220-ms minus relaxed pattern, the intensity increase at 43 nm is closest laterally, the increase at 36 nm is farther out, and the intensity decrease in the 36- to 43-nm region is farthest from the meridian. The layer line increase at 14.3 nm during tension development (better appreciated in Fig. 10, *C* and *D*, than in Fig. 9) has the same lateral spacing as the increase of the 36-nm line. In the 220-ms minus 13-ms difference pattern, the order of lateral positions is different; the increase of intensity at 36 nm is farthest out and the 43-nm increase is intermediate. The net effect is an apparent decrease of intensity at 39 nm close to the meridian. These shifts of the lateral positions suggest that, during final tension development, the cross-bridge mass labeling the long-pitch helix of actin filaments moves progressively toward a smaller radius (closer to the thin filament surface).

DISCUSSION

The average, periodic structures summarized by our computed power density spectra can be compared with x-ray diffraction data obtained from living muscle, and the images provide direct structural information regarding individual sarcomeres and cross-bridges. The computed power spectra are similar to x-ray diffraction patterns from relaxed, rigor, and active muscle (Huxley and Brown, 1967; Haselgrove, 1973; Huxley, 1973; Magid and Reedy, 1980; Padrón and Huxley, 1984; Yagi and Matsubara, 1989; Wakabayashi et al., 1991; Wakabayashi and Amemiya, 1991; Yagi, 1991; Bordas et al., 1993), indicating that structural details are preserved quite well during freezing, processing, and image capture as demonstrated in other studies using the freeze-substitution technique (Nassar et al., 1986; Padrón et al., 1988; Craig et al., 1992; Lenart et al., 1993; Hirose et al., 1993, 1994; Sosa et al., 1994; Hawkins and Bennett, 1995).

Major advantages of our approach are that direct visualization of individual sarcomeres and cross-bridges allows variations from periodic arrangements to be detected. The sharp power density spectra obtained here, excluding data from regions outside the filament overlap zones and summing accurately scaled and aligned patterns, make detection and resolution of some of the layer lines more obvious than in x-ray diffraction patterns, allowing us to detect changes in their intensities and positions. In interpreting the data, however, we need to allow for the possibility that artifacts from freezing, processing, and image capture may alter the structure of the samples from that present at the time of freezing. The x-ray diffraction technique is sensitive directly to excess of protein density over water in the live muscle, so quantitative comparisons of intensities, taking into account instrumental resolution and orientational disorder are, presumably, more reliable than data from electron microscopy.

The changes observed here are consistent with labeling of the long-pitch actin helix by active cross-bridges that tend to be more perpendicular to the fiber axis than rigor cross-bridges. The average mass of attached cross-bridges apparently shifts inward toward smaller radius around the thin filament axis during tension development.

Preservation of relaxed cross-bridge arrangement by freeze substitution

The helical arrangement of myosin heads on the surface of the relaxed myosin is quite labile, particularly in the case of vertebrate muscle (Wray, 1987; Wakabayashi et al., 1988; Lowy et al., 1991; Craig et al., 1992), but it can be preserved with special care (Kensler and Levine, 1982; Stewart and Kensler, 1986; Cantino and Squire, 1986; Ip and Heuser, 1983). The elusive helical tracks are clearly visible in our images, and helical order is demonstrated by oblique striping in thicker sections. In diffraction patterns of relaxed A bands, layer lines and meridional spots are present up to the sixth order of the 43-nm myosin filament repeat, corresponding to resolution of periodic structures to 7.2 nm.

Cross-bridge structure in pre-flash controls compared with relaxed fibers

In unphotolyzed caged Ca^{2+} solution, considerably more of the myosin heads splay out from the surface of the thick filaments than in fibers held in the relaxing solution. Four

points argue that this is not a direct result of an interaction with the thin filaments before photolysis. 1) Splaying of myosin heads occurs in the H zone as well as in the overlap region. 2) The pre-flash fibers develop little or no tension. 3) The in-phase stiffness measured with 2 kHz length oscillations does not increase (T. St. Claire Allen, R. J. Barsotti, and Y. E. Goldman, personal communication). 4) Diffraction patterns and power spectra from the pre-flash controls are dominated by the thick filament periodicities, although the intensity is decreased relative to relaxed fibers.

In our experiments, temperature, ionic strength, and concentration of ATP were approximately equivalent in pre-flash and relaxing solutions, but free $[Mg^{2+}]$ was decreased from ~1 mM to ~50 μM and free $[Ca^{2+}]$ was increased from $<10^{-9}$ M to ~250 nM, so that the fibers were poised at the threshold for contraction. Splaying out of the myosin heads in the pre-flash control may be due to either the lower free Mg^{2+} or higher free Ca^{2+}, and other groups have observed this effect under conditions of lowered divalent cation concentration (Ueno and Harrington, 1981; Ueno et al., 1983; Reisler et al., 1983; Persechini and Rowe, 1984). In rabbit muscle, phosphorylation of the myosin regulatory light chain disorders the cross-bridges in isolated thick filaments (Levine et al., 1995). Liberation of myosin heads from the filament surface has been proposed to underlie potentiation of tension in muscle fibers after phosphorylation of the light chains (Sweeney et al., 1994). Given the brief extraction time of our protocol, it is possible that activation of a calcium-dependent kinase still present in the fibers leads to the myosin head disorder seen in the pre-flash control images.

Cross-bridges in rigor and contracting fibers

The cross-bridges in the two states are clearly distinguishable. In rigor the cross-bridges have an overall tilt toward the Z lines, giving a false impression of arrowheads, and small domains of 36-nm periodicity (see also Varriano-Marston et al., 1984; Craig et al., 1992; Sosa et al., 1994; Hirose et al., 1993, 1994). Images of fibers frozen 13, 34, and 220 ms after Ca^{2+} release are remarkably similar to each other in the overlap region with cross-bridges that are structurally more variable than in either rigor or relaxation. Three general points are worth emphasizing because they are relevant to the discussion of the diffraction patterns that follows. 1) Cross-bridges of activated fibers are of fairly uniform density across the interfilament space, suggesting that they represent single heads (see Bard et al., 1987; Hirose et al., 1994). They display a variety of angles, but a large proportion of them are perpendicular to the filament axis (see also Hirose et al., 1993, 1994). 2) At all time points, A bands and H zones are delimited by sharp edges, indicating good lateral filament alignment, especially at early time points. 3) The prominent transverse lines crossing the whole sarcomere with 43-nm spacing in relaxed fibers are not detectable in active or rigor fibers.

In the H zone, some of the thick filament helical periodicity remains at 13 ms but is lost at later time points. Thus, in contracting muscle, the myosin heads are released from their relaxed position on the thick filament surface even if they do not interact with thin filaments (see also comments on pre-flash fibers). This conclusion disagrees with a careful x-ray diffraction study of muscles at long lengths, which suggested that filament overlap is necessary for alteration of the disposition of myosin heads during contraction (Yagi and Matsubara, 1980). A cooperative effect of activation in the overlap region on head position in the H zone may explain our results.

Myosin-based intensities

The 14.3-nm meridional spot, representing the subunit axial repeat of myosin molecules and also sensitive to cross-bridge tilt (Irving et al., 1992), is stronger in power spectra from rigor and fully contracting muscles than in spectra from relaxed sarcomeres. In x-ray diffraction experiments, this reflection is stronger in contraction but not in rigor (Huxley et al., 1980, 1982; Wakabayashi et al., 1991; Wakabayashi and Amemiya, 1991; Harford and Squire, 1990; Harford et al., 1991). The 43-nm layer line and its second order at 22 nm, which arise from the three-stranded helical architecture of the thick filament defining the origin of myosin heads on the filament surface (Haselgrove, 1983), are present in relaxed and contracting muscle, but not in rigor. The following interpretation of these changes is consistent with the EM images of the various states.

In the relaxed muscle, the myosin heads lie down on the filament shaft at an oblique angle relative to the filament axis (Kensler and Levine, 1982; Kensler and Stewart, 1983; Cantino and Squire, 1986; Ip and Heuser, 1983; Crowther et al., 1985; this paper). Even though the mass of the heads is periodic at 14.3 nm, the oblique orientation spreads the mass of the head in the axial direction, reducing the contrast for scattering into the 14.3-nm spot, as modeled by Haselgrove (1980). In rigor, all cross-bridges are attached to actin, but the intense 14.3-nm reflection indicates that some portion of the myosin head, presumably the head-rod junction, retains the axial 14.3-nm character defined by the polymer structure of backbone. The rest of the head has an overall slightly tilted configuration, with a superimposed variation due to attachment to the target zones of the incommensurate actin lattice (Taylor et al., 1984). Thus, the contribution of myosin heads in rigor to the 14.3-nm periodicity is stronger than in relaxed muscle but not as strong as it would be if all heads were projecting at right angles from the thick filament surface.

In the early part of contraction, the 14.3-nm meridional intensity is greatly reduced, as reported in x-ray diffraction experiments by Huxley et al. (1982), indicating that unattached cross-bridges, and perhaps those in the initial attached states, are too disordered to contribute 14.3-nm periodicity. As tension develops, the 14.3-nm spot again

becomes stronger (Huxley et al., 1982), indicating that attached, perhaps tension-bearing, cross-bridges regain more order at their origin on the thick filament, as do rigor cross-bridges. The number of attached cross-bridges in isometrically contracting muscles is estimated to be 20–80% of that in rigor (Matsubara et al., 1975; Goldman and Simmons, 1977; Cooke et al., 1982; Duong and Reisler, 1989), whereas the 14.3-nm meridional spot is comparable in rigor and active contraction. If fewer cross-bridges are attached and the detached ones contribute little to the 14.3-nm intensity, then the intensity per attachment is greater in contraction. From this, one would predict an overall more perpendicular attitude of the cross-bridges in active than in rigor muscle, as directly observed in the micrographs (Figs. 6 and 7).

The intensities of the myosin layer lines at 43 and 22 nm decrease dramatically at the onset of contraction, in agreement with x-ray diffraction data (Huxley et al., 1980, 1982; Yagi et al., 1981). This initial drop does not seem to be caused by disorder of filament positions, which are well aligned in the images. The 43-nm layer line is due to the helical arrangement of the S1 heads on the surface of the thick filament. The 22-nm forbidden meridional spot is the second order of 43 nm and indicates a two-fold perturbation of the three-stranded thick filament helix because it would not appear from a helix with pure three-fold symmetry (Haselgrove, 1983). Thus, our data indicate a loss of the helical arrangement and the two-fold perturbation. At later stages of contraction, and particularly under maximal tension (220 ms), both 43- and 22-nm myosin layer lines are clearly detectable, suggesting that heads find actin targets while protruding perpendicularly from the filament surface and retaining the thick filament helical character. In x-ray diffraction studies, the off-meridional myosin layer lines retain significant intensity but do not recover toward the relaxed intensities during the rise of tension, a significant discrepancy from the current results.

Actin-based intensities

The first actin and myosin layer lines, at 36 and 43 nm, show up as discrete intensities in our summed power density spectra of contracting muscles. The two layer lines are also distinct in individual optical diffraction patterns from the same fibers (Fig. 5 in Lenart et al., 1993). The 36-nm layer line is sensitive to cross-bridge decoration of target zones arrayed on the long-pitch actin helix. The growth of this layer line, starting 13 ms after photolysis of caged Ca^{2+}, indicates progressive cross-bridge attachment to actin. It is not clear why it is located at 38 nm in fibers frozen 13 ms after activation but at 36 nm at later time points and in rigor. An increase in the intensity of the 5.9-nm layer line has also been attributed to cross-bridge interaction (Matsubara et al., 1984; Wakabayashi et al., 1991) and confirmed by electron microscopy in freeze-substituted contracting muscle (Sosa et al., 1994; Hirose et al., 1994).

The intensity of the 36- to 37-nm actin layer line during contraction has been very difficult to determine by x-ray diffraction, due to the diffuse nature of the neighboring myosin 43-nm layer line. Cross-bridge attachment should increase the intensity, but movement of tropomyosin during activation tends to reduce the 36-nm layer line intensity (Yagi, 1991; Harford and Squire, 1992). Wakabayashi et al. (1991) and Yagi (1991) attempted to resolve this problem by careful deconvolution of the intensity in the 36- to 43-nm axial region at lateral positions either where rigor muscles show a strong intensification (12.5–50 nm) or where the actin layer line peaks at rest (5.5–12.5 nm). The results of this analysis have been contradictory; the deconvolutions gave either a decrease (Wakabayashi et al., 1991) or increase (Yagi, 1991) of the intensity assigned to actin during contraction.

Tsukita and Yano (1985) reported a strong 36-nm layer line in contracting rabbit muscles that were frozen and freeze substituted. However, the contractions lasted for longer periods than here, and a region depleted of ATP may have developed in the core of the muscle bundles. Their images show many angled cross-bridges pointing toward the M line as in rigor, consistent with this possibility. On the other hand, Hirose et al. (1993) showed clearly separate 36- and 43-nm layer lines in optical diffraction patterns from EMs of rabbit fibers activated for very brief times (50 and 80 ms) by photolysis of caged ATP. In that study the fibers started from rigor, so the 36-nm layer line was present throughout the transient, whereas the myosin 43-nm layer line intensified with time, but at time points other than 50 and 80 ms, the data were not sufficient to determine whether both lines were present.

In all of these freeze-substitution studies, the possibility should be considered that the 36-nm layer line is enhanced by association of myosin heads with the thin filament during the freeze-substitution step. Against this possibility, the actin layer line is visible in active fibers freeze substituted both in the absence (Hirose et al., 1993) and presence (this paper) of tannic acid, an agent that greatly improves structural preservation with chemical fixation (Reedy et al., 1983). Hirose et al. (1994) detected the kinetics of shape changes and radial distribution of cross-bridge mass in cross sections of rabbit fibers frozen during activation from rigor by photolysis of caged ATP. If mass of detached cross-bridges artifactually collapses on to the actin periodicity during processing of the samples, it seems unlikely that these major shape changes of attached cross-bridges would be observed. Thus, we consider it unlikely that the presence of the 37-nm layer line in the power spectra (Fig. 9 *F*) is an artifact introduced during processing of the muscle fibers for electron microscopy.

Why is this layer line so intense compared with the corresponding reflection in x-ray diffraction patterns? Most likely, cross-bridges associated with actin at the time of freezing, but too disordered to contribute to the x-ray pattern, are altered during the EM processing in a way that enhances their periodicity. Internal structural changes in

these cross-bridges or their relationship with actin might have this effect. The same phenomenon may also explain the enhancement of the myosin-based off-meridional layer lines during force development. If this explanation is correct, then the strength of the 36-nm layer line obtained here indicates the presence of many cross-bridges, probably weakly attached and structurally disordered but marking actin target zones, during steady contraction. The proportion of cross-bridges in this state increases gradually during development of tension.

As active sarcomeres show evidence for both myosin- and actin-based periodicities, particularly at the peak of tension, one would expect to detect a layer line at 24 nm, as in rigor. The 24-nm spacing arises from the actin 36-nm periodicity convoluted with the axial 14.3-nm spacing of myosin molecules along the thick filament (1/24 nm $\approx$ 1/14.3 − 1/36 nm) and such an actomyosin layer line has been observed in recent two-dimensional x-ray diffraction patterns of contracting muscle (Bordas et al., 1993). The 24-nm layer line is probably hidden in the background scatter in our power spectra from active muscle.

Other reflections, attributable to accessory proteins

The increase in the second thin-filament-based layer line at 18 nm in activated muscle has been attributed to changes associated with a movement of tropomyosin toward the groove of the long-pitch actin helix (Kress et al., 1986; Yagi and Matsubara, 1989; Haselgrove, 1973), but it is also sensitive to cross-bridge binding (Wakabayashi et al., 1991; Popp at al., 1991; Bordas et al., 1993). There is a faint 18-nm layer line in rigor and at 220 ms after activation, but the line is not detectable in the relaxed muscle or at 13 or 34 ms after photolysis. Intensity on the meridian at 19 nm is expected from the disposition of troponin, and in x-ray patterns this intensity also increases in contraction. We see a weak 19-nm layer line at 13 ms that strengthens later in contraction. The origin of this intensity is not known.

The complex clusters on the meridian near 43 and 22 nm are due to axial periodicities of myosin and, presumably, accessory proteins in the thick filament. Among the meridional spots present, the one at 43 nm is thought to be mainly caused by C-protein (Rome et al., 1973b), which leads to the strong transverse striping in the EMs (Figs. 2 and 3), and the one close to 38 nm has been assigned to troponin (Rome et al., 1973a). As mentioned earlier, the 22-nm spot is the second order of 43 nm and indicates a two-fold perturbation of the three-stranded thick filament helix. Weakening of both the 22- and 43-nm spots in rigor and contraction indicates changes of the C-protein disposition and disappearance of the two-fold perturbation. These results are consistent with x-ray experiments. The 43-nm meridional spot, however, reappears at 220 ms and in rigor, possibly indicating that the accessory proteins are fairly ordered in the steady active and rigor states. However, in the EMs we do not see the strong cross-banding observed in relaxing solution.

Significance of lateral shifts of actin- and myosin-based layer lines

We interpret lateral distances of the layer line peaks as indications of the radial position of cross-bridge mass with respect to the thick or thin filaments. However, it should be noted that the proposed ordering of attached cross-bridges during processing of the frozen samples, proposed above to explain the higher intensity of the 37- and 43-nm layer lines during contraction here relative to x-ray diffraction spectra, might also affect the radial mass distribution. Also, shifts of filaments in the direction of the fiber axis could cause some of the lateral changes in peak layer line positions by affecting interfilament coherence and the sampling of the layer lines by the filament lattice. There is no independent estimate of the degree of modulation due to this sampling, so conclusions based on the radial spacings are somewhat uncertain.

The observed lateral shift of the 43-nm layer line peak toward the meridian shortly after photorelease of Ca^{2+} (Table 2) is consistent with radial motions of the heads away from the thick filament surface, seen in the micrographs (cf. Figs. 2 and 6). After 13 ms, the slight shift of the 43-nm layer line position away from the meridian may indicate that the region of the myosin molecule that maintains the helical character defined by the thick filament backbone (possibly the light chain region) is closer to the thick filament surface again. The observed intensity increase implies a progressively increasing mass of cross-bridges settling onto the myosin helical net. In the rigor pattern, the 43-nm layer line is not separate from the 36-nm one, so we do not have reliable information on the lateral position of the myosin layer line in rigor.

Changes in the peak intensity and position of the 36-nm layer line are dramatic and clearly accompany tension development. Assuming that these results are not artifacts due to lattice sampling along the layer line, they suggest that the average radial distance of cross-bridge mass from the center of the actin filaments decreases during force development and is approximately equal at maximal tension and in rigor. This interpretation is consistent with the high fraction of cross-bridges that are closely apposed and slewed tightly around the actin filaments observed in rabbit muscle during late tension development and in rigor (Hirose et al., 1994).

The present experiments supplement x-ray diffraction experiments on live frog muscle in steady states and during the onset of tetanic stimulation. Although there are some considerable differences, many features of the computed power density spectra of our EMs are similar to the corresponding x-ray diffraction spectra. The strong myosin layer lines present in relaxation result from helical tracks of myosin heads directly observed in the EMs. Preservation of these tracks helps to validate the structural preservation

achieved. Upon activation, both electron microscopy and x-ray diffraction show initial weakening of meridional intensities attributable to the axial periodicity of the myosin heads and later intensification and lateral broadening of the 14.3-nm meridional spot. Myosin layer lines recorded with both techniques initially weaken, but then the 43-nm layer line obtained here becomes relatively stronger than the corresponding x-ray layer line late during tension development. The actin layer line at 37 nm in our spectra is much stronger during contraction than in relaxation, whereas in x-ray diffraction patterns it is hardly intensified. The most likely explanation for these quantitative differences is alteration of the structure of attached cross-bridges during processing for electron microscopy. Taken together, the results suggest that, during steady contraction, many cross-bridges that contribute little to the x-ray diffraction pattern due to structural inhomogeneity, are nevertheless associated with actin at the target zones determined by the thin filament helix and retain considerable myosin-based order. Whether this group of variably shaped attachments contributes to force or stiffness is not known.

The work was supported by National Institutes of Health grant HL15835 to the Pennsylvania Muscle Institute and by the Muscular Dystrophy Association.

Dr. Keiko Hirose's contributions to development of the freezing techniques and her continuing suggestions and discussions have been invaluable. We thank Dr. R. Levine for suggesting the possibility of phosphorylation in the pre-flash fibers and Drs. M. K. Reedy and H. E. Huxley for helpful comments and ideas on earlier versions of the manuscript. We thank Drs. J.H. Kaplan and G.C.R. Ellis-Davies for supplying DM-nitrophen. We also thank Mr. Joseph Pili for expert construction of freezing heads with ever-increasing complexity and refinement. Dr. Xin-Hui Sun and Mrs. Nosta Glaser contributed excellent technical and photographic work.

This work was supported by National Institutes of Health grant HL15835 to the Pennsylvania Muscle Institute and by the Muscular Dystrophy Association.

REFERENCES

Amemiya, Y., K. Wakabayashi, H. Tanaka, Y. Ueno, and J. Miyahara. 1987. Laser-stimulated luminescence used to measure x-ray diffraction of a contracting striated muscle. *Science*. 237:164–168.

Bard, F., C. Franzini-Armstrong, and W. Ip. 1987. Rigor crossbridges are double-headed in fast muscle from crayfish. *J. Cell Biol.* 105: 2225–2234.

Bennett, P., R. Craig, R. Starr, and G. Offer. 1986. The ultrastructural location of C-protein, X-protein, and H-protein in rabbit muscle. *J. Muscle Res. Cell Motil.* 7:550–567.

Bordas, J., G. P. Diakun, F. G. Diaz, J. E. Harries, R. A. Lewis, J. Lowy, G. R. Mant, M. L. Martin-Fernandez, and E. Towns-Andrews. 1993. Two-dimensional time-resolved x-ray diffraction studies of live isometrically contracting frog sartorius muscle. *J. Muscle Res. Cell Motil.* 14:311–324.

Bordas, J., G. P. Diakun, J. E. Harries, R. A. Lewis, G. R. Mant, M. L. Martin-Fernandez, and E. Towns-Andrews. 1991. Two-dimensional time resolved x-ray diffraction of muscle: recent results. *Adv. Biophys.* 27:15–33.

Brenner, B., M. A. Ferenczi, M. Irving, R. M. Simmons, and E. Towns-Andrews. 1989. Myosin cross-bridge movement observed by time-resolved x-ray diffraction in a single permeabilized fibre isolated from frog muscle. *J. Physiol.* 415:113P.

Cantino, M., and J. Squire. 1986. Resting myosin cross-bridge configuration in frog muscle thick filaments. *J. Cell Biol.* 102:610–618.

Cooke, R., M. S. Crowder, and D. D. Thomas. 1982. Orientation of spin labels attached to cross-bridges in contracting muscle fibres. *Nature*. 300:776–778.

Craig, R., L. Alamo, and R. Padrón. 1992. Structure of the myosin filaments of relaxed and rigor vertebrate striated muscle studied by rapid freezing electron microscopy. *J. Mol. Biol.* 228:474–487.

Craig, R., and G. Offer. 1976. The location of C-protein in rabbit skeletal muscle. *Proc. Roy. Soc. Ser. B.* 192:451–461.

Crowther, R. A., R. Padrón, and R. Craig. 1985. Arrangement of the heads of myosin in relaxed thick filaments from tarantula muscle. *J. Mol. Biol.* 184:429–439.

Duong, A. M., and E. Reisler. 1989. Binding of myosin to actin in myofibrils during ATP hydrolysis. *Biochemistry*. 28:1307–1313.

Goldman, Y. E., M. G. Hibberd, and D. R. Trentham. 1984. Relaxation of rabbit psoas muscle fibres from rigor by photochemical generation of adenosine-5′-triphosphate. *J. Physiol.* 354:577–604.

Goldman, Y. E., and R. M. Simmons. 1977. Active and rigor muscle stiffness. *J. Physiol.* 269:55–57P.

Goldman, Y. E., and R. M. Simmons. 1984. Control of sarcomere length in skinned muscle fibres of *Rana temporaria* during mechanical transients. *J. Physiol.* 350:497–518.

Hanson, J., and H. E. Huxley. 1955. The structural basis of contraction in striated muscle. *Symp. Soc. Exp. Biol.* 9:228–264.

Harford, J. J., M. W. Chew, J. M. Squire, and E. Towns-Andrews. 1991. Crossbridge states in isometrically contracting fish muscle: evidence for swinging of myosin heads on actin. *Adv. Biophys.* 27:45–61.

Harford, J., and J. M. Squire. 1990. Static and time-resolved x-ray diffraction studies of fish muscle. *In* Molecular Mechanisms in Muscular Contraction. J. M. Squire, editor. CRC Press, Boca Raton, FL. 287–320.

Harford, J. J., and J. M. Squire. 1992. Evidence for structurally different attached states of myosin cross-bridges on actin during contraction of fish muscle. *Biophys. J.* 63:387–396.

Haselgrove, J. C. 1973. X-ray evidence for a conformational change in the actin-containing filaments of vertebrate striated muscle. *Cold Spring Harbor Symp. Quant. Biol.* 37:341–352.

Haselgrove, J. C. 1980. A model of myosin crossbridge structure consistent with the low-angle x-ray diffraction pattern of vertebrate muscle. *J. Muscle Res. Cell Motil.* 1:177–191.

Haselgrove, J. C. 1983. Structure of vertebrate striated muscle as determined by x-ray diffraction studies. *In* Handbook of Physiology. L. D. Peachey, editor. Williams & Wilkins, Baltimore. 143–171.

Haselgrove, J. C., and H. E. Huxley. 1973. X-ray evidence for radial cross-bridge movement and for the sliding filament model in actively contracting skeletal muscle. *J. Mol. Biol.* 77:549–568.

Hawkins, C. J., and P. M. Bennett. 1995. Evaluation of freeze substitution in rabbit skeletal muscle: comparison of electron microscopy to x-ray diffraction. *J. Muscle Res. Cell Motil.* 16:303–318.

Heuser, J. E., and R. Cooke. 1983. Actin-myosin interactions visualized by the quick-freeze, deep-etch replica technique. *J. Mol. Biol.* 169:97–122.

Heuser, J. E., T. S. Reese, M. J. Dennis, Y. Jan, L. Jan, and L. Evans. 1979. Synaptic vesicle exocytosis captured by quick freezing and correlated with quantal transmitter release. *J. Cell Biol.* 81:275–300.

Hirose, K., C. Franzini-Armstrong, Y. E. Goldman, and J. M. Murray. 1994. Structural changes in muscle cross-bridges accompanying force generation. *J. Cell Biol.* 127:763–778.

Hirose, K., T. D. Lenart, J. M. Murray, C. Franzini-Armstrong, and Y. E. Goldman. 1993. Flash and smash: rapid freezing of muscle fibers activated by photolysis of caged ATP. *Biophys. J.* 65:397–408.

Hirose, K., and T. Wakabayashi. 1991. Conformations of crossbridges in contracting skeletal muscle. *Adv. Biophys.* 27:197–203.

Holmes, K. C., D. Popp, W. Gebhard, and W. Kabsch. 1991. Atomic model of the actin filament. *Nature*. 347:44–45.

Huxley, A. F. 1957. Muscle structure and theories of contraction. *Prog. Biophys. Biophys. Chem.* 7:255–318.

Huxley, H. E. 1969. The mechanism of muscular contraction. *Science*. 164:1356–1366.

Huxley, H. E. 1973. Structural changes in the actin- and myosin-containing filaments during contraction. *Cold Spring Harbor Symp. Quant. Biol.* 37:361–378.

Huxley, H. E., and W. Brown. 1967. The low-angle x-ray diagram of vertebrate striated muscle and its behaviour during contraction and rigor. *J. Mol. Biol.* 30:383–434.

Huxley, H. E., A. R. Faruqi, J. Bordas, M. H. J. Koch, and J. R. Milch. 1980. The use of synchrotron radiation in time-resolved x-ray diffraction studies of myosin layer-line reflections during muscle contraction. *Nature.* 284:140–143.

Huxley, H. E., A. R. Faruqi, M. Kress, J. Bordas, and M. H. J. Koch. 1982. Time-resolved x-ray diffraction studies of the myosin layer-line reflections during muscle contraction. *J. Mol. Biol.* 158:637–684.

Huxley, H. E., and M. Kress. 1985. Crossbridge behaviour during muscle contraction. *J. Muscle Res. Cell Motil.* 6:153–161.

Huxley, H. E., R. M. Simmons, A. R. Faruqi, M. Kress, J. Bordas, and M. H. J. Koch. 1981. Millisecond time-resolved changes in x-ray reflections from contracting muscle during rapid mechanical transients, recorded using synchrotron radiation. *Proc. Natl. Acad. Sci. USA.* 78:2297–2301.

Ip, W., and J. Heuser. 1983. Direct visualization of the myosin crossbridge helices on relaxed rabbit psoas thick filaments. *J. Mol. Biol.* 171: 105–109.

Irving, M., V. Lombardi, G. Piazzesi, and M. A. Ferenczi. 1992. Myosin head movements are synchronous with the elementary force-generating process in muscle. *Nature.* 357:156–158.

Kaplan, J. H., and G. C. R. Ellis-Davies. 1988. Photolabile chelators for the rapid photorelease of divalent cations. *Proc. Natl. Acad. Sci. USA.* 85:6571–6575.

Kensler, R. W., and R. J. C. Levine. 1982. An electron microscopic and optical diffraction analysis of the structure of *Limulus* telson muscle thick filaments. *J. Cell Biol.* 92:443–451.

Kensler, R. W., and M. Stewart. 1983. Frog skeletal muscle thick filaments are three-stranded. *J. Cell Biol.* 96:1797–1802.

Kensler, R. W., and M. Stewart. 1986. An ultrastructural study of cross-bridge arrangement in the frog thigh muscle thick filament. *Biophys. J.* 49:343–351.

Kensler, R. W., and M. Stewart. 1989. An ultrastructural study of cross-bridge arrangement in the fish skeletal muscle thick filament. *J. Cell Sci.* 94:391–401.

Kress, M., H. E. Huxley, A. R. Faruqi, and J. Hendrix. 1986. Structural changes during activation of frog muscle studied by time-resolved x-ray diffraction. *J. Mol. Biol.* 188:325–342.

Lenart, T. D., T. St. Claire Allen, R. J. Barsotti, G. C. R. Ellis-Davies, J. H. Kaplan, C. Franzini-Armstrong, and Y. E. Goldman. 1993. Mechanics and structure of cross-bridges during contractions initiated by photolysis of caged Ca^{2+}. *In* Mechanism of Myofilament Sliding in Muscle Contraction. H. Sugi and G. H. Pollack, editors. Plenum Press, New York. 475–487.

Lenart, T. D., C. Franzini-Armstrong, and Y. E. Goldman. 1992. Ultrastructure of frog sartorius muscle fibers quickly frozen following activation by caged Ca^{2+} photolysis. *Biophys. J.* 61:A286.

Levine, R. J. C., R. W. Kensler, Z. Yang, and H. L. Sweeney. 1995. Myosin regulatory light chain phosphorylation and the production of functionally significant changes in myosin head arrangement on striated muscle thick filaments. *Biophys. J.* 68:224s.

Lowy, J., D. Popp, and A. A. Stewart. 1991. X-ray studies of order-disorder transitions in the myosin heads of skinned rabbit psoas muscles. *Biophys. J.* 60:812–824.

Magid, A., and M. K. Reedy. 1980. X-ray diffraction observations of chemically skinned frog skeletal muscle processed by an improved method. *Biophys. J.* 30:27–40.

Matsubara, I., N. Yagi, and H. Hashizume. 1975. Use of an x-ray television for diffraction of the frog striated muscle. *Nature.* 255:728–729.

Matsubara, I., N. Yagi, H. Miura, M. Ozeki, and T. Izumi. 1984. Intensification of the 5.9-nm actin layer line in contracting muscle. *Nature.* 312:471–473.

Milligan, R. A., M. Whittaker, and D. Safer. 1990. Molecular structure of F-actin and location of surface binding sites. *Nature.* 348:217–221.

Murray, J. M., T. D. Lenart, C. Franzini-Armstrong, and Y. E. Goldman. 1993. Structural changes in cross-bridges of skinned muscle fibers activated by photolysis of caged Ca^{2+} and rapidly frozen for electron microscopy. *Biophys. J.* 64:A26.

Nassar, R., N. R. Wallace, I. Taylor, and J. R. Sommer. 1986. The quick-freezing of single intact skeletal muscle fibers at known time intervals following electrical stimulation. *Scanning Electron Microsc.* I:309–328.

Padrón, R., L. Alamo, R. Craig, and C. Caputo. 1988. A method for quick-freezing live muscles at known instants during contraction with simultaneous recording of mechanical tension. *J. Microsc.* 151: 81–102.

Padrón, R., and R. Craig. 1989. Disorder induced in nonoverlap myosin cross-bridges by loss of adenosine triphosphate. *Biophys. J.* 56:927–933.

Padrón, R., and H. E. Huxley. 1984. The effect of the ATP analogue AMPPNP on the structure of crossbridges in vertebrate skeletal muscles: x-ray diffraction and mechanical studies. *J. Muscle Res. Cell Motil.* 5:613–655.

Pepe, F. A., and B. Drucker. 1975. The myosin filament. III. C-protein. *J. Mol. Biol.* 99:609–617.

Persechini, A., and A. J. Rowe. 1984. Modulation of myosin filament conformation by physiological levels of divalent cation. *J. Mol. Biol.* 172:23–39.

Poole, K. J. V., Y. Maeda, G. Rapp, and R. S. Goody. 1991. Dynamic x-ray diffraction measurements following photolytic relaxation and activation of skinned rabbit psoas fibres. *Adv. Biophys.* 27:63–75.

Popp, D., Y. Maeda, A. A. E. Stewart, and K. C. Holmes. 1991. X-ray diffraction studies on muscle regulation. *Adv. Biophys.* 27:89–103.

Rapp, G., K. J. V. Poole, Y. Maeda, G. C. R. Ellis-Davies, J. H. Kaplan, J. McCray, and R. S. Goody. 1989. Lasers and flashlamps in research on the mechanism of muscle contraction. *Ber. Bunsenges. Phys. Chem.* 93:410–415.

Rayment, I., W. R. Rypniewski, K. Schmidt-Bäse, R. Smith, D. R. Tomchick, M. M. Benning, D. A. Winkelmann, G. Wesenberg, and H. M. Holden. 1993. Three-dimensional structure of myosin subfragment-1: a molecular motor. *Science.* 261:50–58.

Reedy, M. K., K. C. Holmes, and R. T. Tregear. 1965. Induced changes in orientation of the cross-bridges of glycerinated insect flight muscle. *Nature.* 207:1276–1280.

Reisler, E., J. Liu, and P. Cheung. 1983. Role of magnesium binding to myosin in controlling the state of cross-bridges in skeletal rabbit muscle. *Biochemistry.* 22:4954–4960.

Rome, E. M., T. Hirabayashi, and S. V. Perry. 1973a. X-ray diffraction of muscle labelled with antibody to troponin-C. *Nature New Biol.* 244: 154–155.

Rome, E. M., G. Offer, and F. A. Pepe. 1973b. X-ray diffraction of muscle labelled with antibody to C-protein. *Nature New Biol.* 244:152–154.

Sosa, H., D. Popp, G. Ouyang, and H. E. Huxley. 1994. Ultrastructure of skeletal muscle fibers studied by a plunge quick freezing method: myofilament lengths. *Biophys. J.* 67:283–292.

Stewart, M., and R. W. Kensler. 1986. Arrangement of myosin heads in relaxed thick filaments from frog skeletal muscle. *J. Mol. Biol.* 192: 831–851.

Suzuki, S., Y. Oshimi, and H. Sugi. 1993. Freeze-fracture studies on the cross-bridge angle distribution at various states and the thin filament stiffness in single skinned frog muscle fibers. *J. Electron Microsc.* 42:107–116.

Sweeney, H. L., Z. Yang, G. Zhi, J. T. Stull, and K. M. Trybus. 1994. Charge replacement near the phosphorylatable serine of the myosin regulatory light chain mimics aspects of phosphorylation. *Proc. Natl. Acad. Sci. USA.* 91:1490–1494.

Taylor, K. A., M. C. Reedy, L. Córdova, and M. K. Reedy. 1984. Three-dimensional reconstruction of rigor insect flight muscle from tilted thin sections. *Nature.* 310:285–291.

Tsukita, S., and M. Yano. 1985. Actomyosin structure in contracting muscle detected by rapid freezing. *Nature.* 317:182–184.

Tsukita, S., and M. Yano. 1986. The ultrastructure of contracting skeletal muscle: a freeze-substitution and freeze-etch replica study. *In* Cell

Motility: Mechanisms and Regulation. H. Ishikawa, S. Hatano, and H. Sato, Tokyo Press, Tokyo. 77–87.

Ueno, H., and W. F. Harrington. 1981. Cross-bridge movement and the conformational state of the myosin hinge in skeletal muscle. *J. Mol. Biol.* 149:619–640.

Ueno, H., M. E. Rodgers, and W. F. Harrington. 1983. Self-association of a subfragment-2 of myosin induced by divalent metal ions. *Biophys. J.* 41:A230.

Varriano-Marston, E., C. Franzini-Armstrong, and J. C. Haselgrove. 1984. The structure and disposition of crossbridges in deep-etched fish muscle. *J. Muscle Res. Cell Motil.* 5:363–386.

Wakabayashi, K., and Y. Amemiya. 1991. Progress in x-ray synchrotron diffraction studies of muscle contraction. *In* Handbook on Synchrotron Radiation. S. Ebashi, M. Koch, and E. Rubenstein, editors. Elsevier Science Publishers, New York. 597–678.

Wakabayashi, K., H. Tanaka, H. Saito, N. Moriwaki, Y. Ueno, and Y. Amemiya. 1991. Dynamic x-ray diffraction of skeletal muscle contraction: structural change of actin filaments. *Adv. Biophys.* 27:3–13.

Wakabayashi, T., T. Akiba, K. Hirose, A. Tomioka, M. Tokunaga, M. Suzuki, C. Toyoshima, K. Sutoh, K. Yamamoto, T. Matsumoto, K. Saeki, and Y. Amemiya. 1988. Temperature-induced change of thick filament and location of the functional sites of myosin. *Adv. Exp. Med. Biol.* 226:39–48.

Wray, J. S. 1987. Structure of relaxed myosin filaments in relation to nucleotide state in vertebrate skeletal muscle. *J. Muscle Res. Cell Motil.* 8:A62.

Xie, X., D. H. Harrison, I. Schlichting, R. M. Sweet, V. N. Kalabokis, A. G. Szent-Györgyi, and C. Cohen. 1994. Structure of the regulatory domain of scallop myosin at 2.8 Å resolution. *Nature.* 368:306–312.

Yagi, N. 1991. Intensification of the first actin layer-line during contraction of frog skeletal muscle. *Adv. Biophys.* 27:35–43.

Yagi, N., M. H. Ito, H. Nakajima, T. Izumi, and I. Matsubara. 1977. Return of myosin heads to thick filaments after muscle contraction. *Science.* 197:685–687.

Yagi, N., and I. Matsubara. 1980. Myosin heads do not move on activation in highly stretched vertebrate striated muscle. *Science.* 207:307–308.

Yagi, N., and I. Matsubara. 1989. Structural changes in the thin filament during activation studied by x-ray diffraction of highly stretched skeletal muscle. *J. Mol. Biol.* 208:359–363.

Yagi, N., E. J. O'Brien, and I. Matsubara. 1981. Changes of thick filament structure during contraction of frog striated muscle. *Biophys. J.* 33: 121–138.